Int J Adv Manuf Technol (2016) 83:1037–1045
DOI 10.1007/s00170-015-7651-8

ORIGINAL ARTICLE

An inverse heat conduction method to determine the energy transferred to the workpiece in EDM process

Mohammadreza Shabgard[1] · **Sina Akhbari**[1]

Received: 12 February 2015 / Accepted: 23 July 2015 / Published online: 5 August 2015

Abstract In this paper, an inverse heat conduction method is applied to estimate the amount of the energy (F_c) transferred to the workpiece during electric discharge machining (EDM) process. Embedded thermocouples which were connected to a four channel data logger were utilized to measure the temperature of a specific location on a rectangular workpiece during the EDM process. After temperature measurements were done, the 2-D heat conduction model of the workpiece and the Levenberg-Marquardt (LM) scheme were used to determine the energy transferred to the workpiece. This inverse procedure facilitates the determination of the heat energy at discharge-workpiece interface in EDM processes, which yet is a challenge for existing numerical models. The obtained results showed that the energy transferred to the workpiece varies with the discharge current and pulse duration from 5 % up to 45 %, which shows that the value of F_c is a function of discharge current and pulse duration and that the fixed value of energy assumed in majority of the previous researches is not in accordance with real EDM conditions. Furthermore, the effects of machining parameters such as discharge current and pulse duration on F_c were studied. It was evident that the F_c has a direct but non-linear relationship with both discharge current and pulse duration, while discharge current has a higher impact on F_c.

✉ Mohammadreza Shabgard
mrshabgard@tabrizu.ac.ir

Sina Akhbari
S_akhbari@tabrizu.ac.ir

[1] Department of Mechanical Engineering, Tabriz University, 29 Bahman Boulevard, Tabriz 51666-14766, Iran

Keywords EDM · Inverse heat conduction · Temperature measurements · Discharge current · Pulse duration · Discharge energy · Point heat source

1 Introduction

Electric discharge machining (EDM) process possesses a complex and stochastic nature. The process involves a combination of several phenomena such as electrodynamics, electromagnetic, thermodynamic, and hydrodynamic [1]. Nonetheless, except for very short discharges, it can be considered with negligible bias that thermal effect is the dominant phenomena [2]. During this process, electrical energy is converted to thermal energy, which is then distributed between the tool and workpiece (designated as electrodes) and the dielectric fluid. However, the only part of the energy transferred to the workpiece is considered as the machining energy and has the dominant impact on material removal rate, crater geometry, and other machining characteristics of EDM process. Therefore, the portion of energy transferred to the workpiece (F_c) is one of the most important parameters in thermal modeling of EDM process. Hence, it is of great importance to determine the energy delivered to the workpiece.

In the past, researchers such as Snoeys [3], Van Dijck [4], Beck [5, 6], Jilani [7], and Pandey [8] assumed the same and constant percentage of energy (F_c=50 %) transferred to cathode and anode, i.e., workpiece and tool, for different machining conditions in their simulation of EDM process. This appeared to be the main reason for the incompatibilities between numerical results and real-time EDM process [9]. Later on, DiBitonto [10] assumed that only a small part of discharge energy

(F_c=18 %) is transferred to cathode and the remaining energy is either transferred to anode or is dissipated to dielectric fluid. Although this assumption improved the theoretical models of EDM process, but due to the fact that same amount of energy was used for different setups, numerical results were still lacking accuracy when compared to experimental results [1].

There are a few studies which have attempted to determine the portion of energy transferred to the workpiece in EDM process with varying machining parameters. Eubank et al [11] developed a comprehensive variable mass, cylindrical plasma model for the EDM spark based on fluid mechanics, thermodynamics, and radiation theories. They concluded that an increase in discharge current and pulse duration results in higher discharge energy. Xia et al [12] measured the energy distribution by comparing the measured temperatures of the electrodes with the calculated results obtained under the assumed portion of the energy distributed in electrodes. They found that when the calculated temperature agreed with the measured one, the estimated energy distribution was correct. Furthermore, they reported that the energy distribution to anode and cathode is about 40 and 25 %, respectively. Joshi and Pande [13] improved the prediction accuracy of their thermo-physical model by varying the values of the portion of discharge energy transferred to the workpiece with current and pulse duration. They concluded that it is essential to apply higher energy distribution factor for higher energy zones. Moreover, they recommended energy distribution factors 0.183 for lower energy zone (up to 100 mJ), while 0.183–0.2 for medium energy zone (100–650 mJ). Singh [14] studied the effect of discharge current and pulse duration on energy received by workpiece in EDM process utilizing thermodynamics principles. His results showed that effective energy conducted to the workpiece depends on applied values of discharge current and pulse duration and it varies from 6.5 to 35 % for different machining conditions. Zahiruddin and Kunieda [15] estimated the percentage of power transferred to the workpiece in micro-EDM process by comparing and fitting the obtained temperature curves from simulation with the experimental temperature curves.

Finally, since there is incompatibility of data in literature and also a lack of a general method of determining F_c in EDM process, this study presents a novel method of calculating the energy received by workpiece utilizing combined experimental and numerical data. This was done through solving the inverse heat conduction problem that exists in EDM process. Furthermore, graphs showing the relationship between F_c and discharge current and pulse duration are presented. In addition, the inverse method described in this work can be utilized to calculate the energy distributed to the tool as well.

Nomenclature

Symbol	Meaning	Units
V	Voltage	v
I_{dis}	Discharge current	A
T_{on}	Pulse duration	μs
F_c	Faction of energy transferred to the W.P	-
K	Thermal conductivity	W/m°C
ρ	Density	Kg/m^3
c_p	Specific heat	J/kg°C
L	Workpiece length	m
X_H	Spatial location of heat source along x direction	m
Y_H	Spatial location of heat source along y direction	m
x_{meas}	Spatial location of embedded thermocouple along x direction	m
y_{meas}	Spatial location of embedded thermocouple along y direction	m
T_∞	Initial temperature	°C
h	Convective heat transfer coefficient	W/m^2°C
$\alpha=K/\rho c_p$	Thermal diffusivity	m^2/s
T	Temperature	°C
Q	Heat source power	W
$\delta(.)$	Dirac delta function	-
i	Spatial step numerator along x axis	-
j	Spatial step numerator along y axis	-
n	Time step numerator	-
Δx	Spatial increment along x direction	m
Δy	Spatial increment along y direction	m
Δt	Time increment	s
$F_0=\alpha\Delta t/\Delta x^2$	Fourier number	-
$Bi=\Delta x h/K$	Biot number	-
P	Unknown power to be estimated	W
$S(P)$	Sum of squares error or objective function	°C
$Y_i=Y(t_i)$	Measured temperature at time t_i	°C
$T_i(P)$	Calculated temperature at t_i from direct problem	°C
k	Numerator of iteration	-
μ	Damping parameter	-
Ω	Diagonal matrix	-
J	Sensitivity matrix	°C/W
E_{total}	Total discharge energy	mJ
E_w	Energy received by the W.P	mJ
P_w	Power transferred to the W.P	W

2 Experiments

Experiments were conducted under varying discharge current and pulse duration whereas other input parameters were held

constant. Table 1 lists the machining conditions and parameter settings used in experiments. As it is listed in this table, four levels for each variable parameters were selected and the experiments were designed utilizing full factorial method.

The material chosen for workpieces and tools used in the experiments were mild steel (st37) and copper, respectively. Table 2 lists the thermo-physical properties of the workpiece. Moreover, Fig. 1 illustrates the schematic configuration of workpiece (as cathode) and tool (as anode). As it is demonstrated in Fig. 1, the workpiece was a thin rectangular plate, which was 50 mm in length and 50 mm in width. Small holes were drilled on the workpiece for embedding the thermocouples. In order to avoid unwanted electromagnetic noises and because thermocouple used in this study could not withstand high voltage, these holes were made 7 mm away from the discharge location [16]. Furthermore, copper tools were designed with a pointy tip as it is apparent in Fig. 1 so that discharges could occur on a fixed location. Moreover, it should be noted that the copper tool has a very high thermal conductivity and has positive polarity and tiny cross section due to small diameter in the body. Accordingly, it conducts the heat through in a very high rate and the erosion from the tool stays very low specifically in long pulse durations; therefore, even in long machining times and erosive machining conditions, the tip of the tool remains almost unscathed. In other words, it is safe to say that, in this research, the discharge location on workpiece surface was made independent of position and time. Lastly, with good approximation, it was assumed to be a constant point heat source [10, 13].

Figure 2 illustrates the experimental setup. As it is shown, four K-Type thermocouples were embedded on specific locations (drilled holes) in order to establish a confident temperature field. Next, these thermocouples were connected to "TES 1384" four channel data logger which was then used for collecting the data sent via thermocouples from the beginning to the end of each experiment . Moreover, thin Teflon pads as insulators were placed between the clamp and workpiece interface so that no conduction to fixtures would occur. Furthermore, the flow of dielectric was constrained within a small chamber. Finally, during each experiment, temperature changes in workpiece at 1-s intervals were recorded by the data logger. Afterwards, the information attained by means of data logger were used in solving the inverse heat transfer problem.

Table 1 Parameter settings and machining conditions

Experimental settings and conditions	Unit	Value
Generator type	-	Iso-pulse
Dielectric fluid	-	Oil
Flushing	-	Normal
Voltage	v	80
Polarity		Positive
Discharge current	A	2, 4, 8, and 12
Pulse duration	μs	12.8, 25, 50, 100
Pulse off-time	μs	6.4
Initial temperature	°C	25

Table 2 Thermo-physical properties of mild steel [17]

Thermal conductivity (k)	50 W/m°C
Density (ρ)	7800 kg/m^3
Specific heat (c_p)	460 J/kg°C

3 Inverse determination of energy transferred to workpiece

Determining an unknown power or energy which causes a specific temperature distribution field in a solid body while other boundary and initial conditions are known, which was the case in current study, is defined as an inverse heat conduction problem [18]. Accordingly, the governing inverse problem is solved and the ratio of energy-power transferred to the workpiece (F_c) is calculated utilizing the Levenberg-Marquardt (LM) technique. The LM is an iterative method for solving nonlinear least squares problems of parameter estimation, which has also been successfully applied to the solution of linear problems that are too ill-conditioned to permit the application of linear algorithms [19].

In this method, first the direct heat conduction model of EDM process is introduced. Then by solving the direct heat problem, temperature distribution in workpiece in terms of unknown power is obtained. Finally, by minimization of the least squares error function defined between measured temperatures and estimated temperatures, the unknown power received by the workpiece is determined.

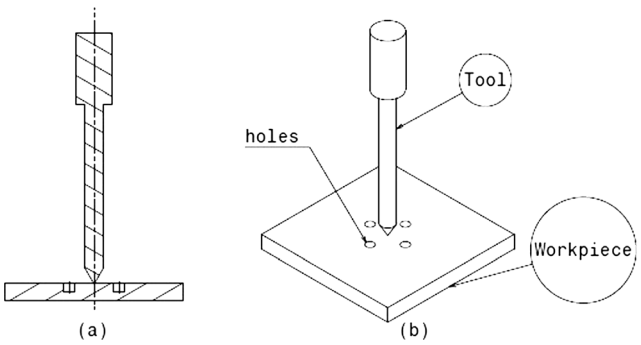

Fig. 1 Schematic diagram of workpiece and tool configuration in **a** 2-D and **b** 3-D

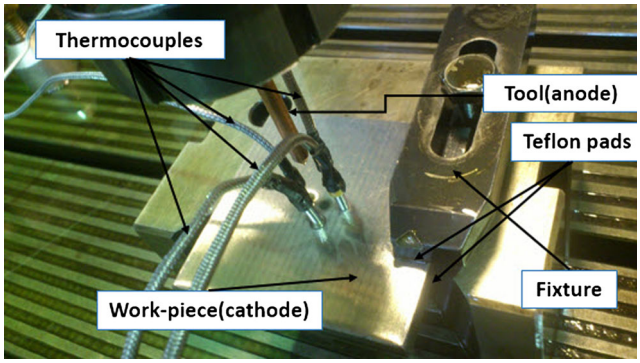

Fig. 2 Experimental setup

3.1 Direct 2-D heat conduction model

As described above, the first step of solving an inverse heat transfer problem is to define its governing heat conduction model. EDM processes utilize electrical discharges which occur between the workpiece as cathode and the tool as anode for material removal. Due to the fact that the heat transferred by conduction is the main phenomenon involved in EDM process, these discharges play the role of the heat source which generates thermal energy. The heat is then transferred to the workpiece by conduction. For simplification purposes and also defining the thermal model along its boundary and initial conditions, the following assumptions were made:

- The workpiece and the dielectric fluid are considered as continuum in numerical computation.
- Workpiece material is homogeneous and isotropic in nature.
- Thermo-physical properties of workpiece are considered to be independent of temperature.
- Due to the workpiece being a rectangular plate in shape with a negligible thickness compared to other dimensions (by ratio of <1/10), two-dimensional heat transfer on *x*-*y* plane in a Cartesian space is presumed [17].
- In EDM process, discharges occur on a fixed location with a very high frequency (20000 ~ 30000 Hz [13]). Also, off-time period is very small compared to on-time period. Plus, during the machining, the tool tip maintains pointy. Therefore, discharges are assumed to be independent of time and position which results in a constant point heat source [20].
- Initial temperature is assumed to be the temperature of dielectric fluid at the beginning of each test.
- Since the workpiece was surrounded by constrained flow of dielectric fluid, the governing boundary conditions were of a convection kind.

Taking these assumptions and conditions into the account, a schematic diagram of 2-D heat transfer phenomenon is illustrated in Fig. 3. Accordingly, the mathematical modeling of EDM process is based on partial differential equations of transient heat conduction with point heat source and boundary conditions of the third type as indicated in Eqs. 1 and 2, respectively. Moreover, Table 3 lists the values of input parameters which define the boundary and initial conditions as depicted in Fig. 3.

$$\frac{\partial T}{\partial t} = \alpha\left(\frac{\partial^2 T}{\partial x^2} + \frac{\partial^2 T}{\partial y^2}\right) + Q\delta(x - x_H)\delta(y - y_H) \tag{1}$$

$$\begin{cases} \pm K\dfrac{\partial T}{\partial x} = h(T - T_\infty) \text{ for } x = 0,\ x = L \\ \pm K\dfrac{\partial T}{\partial y} = h(T - T_\infty) \text{ for } y = 0,\ x = L \\ T(x, y, 0) = T_\infty = 25^\circ\text{C} \end{cases} \tag{2}$$

3.2 Solution of the direct problem

Alternating-direction implicit (ADI) scheme is applied for solving the partial differential in Eq. 1. ADI is a powerful and the most effective finite difference method in solving parabolic PDEs [21]. In this method, each time increment is executed in two half steps: each step is conditionally stable, but "combination of two half steps" is unconditionally stable. In other words, In the first time step, the spatial derivatives in one direction, say *y*, are evaluated at the known time level *n* and the other spatial derivatives, say *x*, are evaluated at the

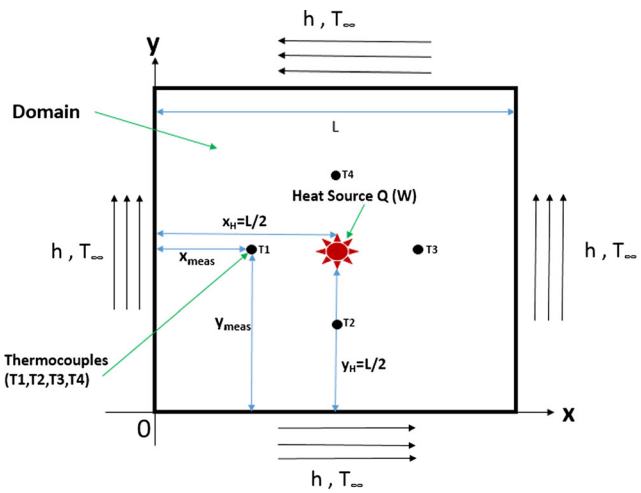

Fig. 3 Schematic diagram of 2-D heat transfer phenomenon which occurs in EDM process

Table 3 Values of parameters used in defining conditions of thermal model

Parameter	Value
L	50 mm
X_H=Y_H	25 mm
x_{meas}(T1)	18 mm
y_{meas}(T1)	25 mm
x_{meas}(T2)	25 mm
y_{meas}(T2)	18 mm
x_{meas}(T3)	32 mm
y_{meas}(T3)	25 mm
x_{meas}(T4)	25 mm
y_{meas}(T4)	32 mm
T_∞	25 °C
k	50 W/m°C
h	10,000 W/m^2°C

unknown time level $n+1$. On the next time step, the process is reversed. Assuming the spatial increments to be equal ($\Delta x=\Delta y$), the discretized equations for internal grids are obtained as depicted in Eq. 3:

$$\begin{cases} -F_0T_{i,j-1}^{n+\frac{1}{2}}+(2+2F_0)T_{i,j}^{n+\frac{1}{2}}-F_0T_{i,j+1}^{n+\frac{1}{2}}=F_0T_{i-1,j}^{n+\frac{1}{2}}+(2-2F_0)T_{i,j}^{n+\frac{1}{2}} \\ +F_0T_{i+1,j}^{n+\frac{1}{2}}+\Delta tQ\delta(x_i-x_H)\delta\left(y_j-y_H\right) \\ -F_0T_{i-1,j}^{n+1}+(2+2F_0)T_{i,j}^{n+1}-F_0T_{i+1,j}^{n+1}=F_0T_{i,j-1}^{n+\frac{1}{2}}+(2-2F_0)T_{i,j}^{n+\frac{1}{2}} \\ +F_0T_{i,j+1}^{n+\frac{1}{2}}+\Delta tQ\delta(x_i-x_H)\delta\left(y_j-y_H\right) \end{cases} \tag{3}$$

Afterwards, the boundary and initial conditions indicated in Eq. 2 are discretized and shown in Eq. 4:

$$\begin{cases} K\dfrac{T_2^n-T_0^n}{2\Delta x}=h\left(T_1^n-T_\infty\right)\overset{\frac{\Delta xh}{K}=Bi}{\rightarrow}T_0^n=T_2^n-2Bi\left(T_1^n-T_\infty\right) \\ -K\dfrac{T_{m+1}^n-T_{m-1}^n}{2\Delta x}=h\left(T_m^n-T_\infty\right)\overset{\frac{\Delta xh}{K}=Bi}{\rightarrow}T_{m+1}^n=T_{m-1}^n-2Bi\left(T_m^n-T_\infty\right) \\ T_{i,j}^0=T_\infty=25\mathring{A}\text{C} \end{cases} \tag{4}$$

Next, discretized terms in Eq. 4 are placed in the main finite differences in Eq. 3 and the finite difference equations for the grids located on boundaries of the domain are obtained and indicated in Eq. 5:

$$\begin{cases} i=1,j=1\rightarrow(2+2F_0(1+Bi))T_{1,1}^{n+\frac{1}{2}}-2F_0T_{1,2}^{n+\frac{1}{2}}=(2-2F_0(1+Bi))T_{1,1}^n+2F_0T_{2,1}^n+4F_0BiT_\infty \\ i>1,j=1\rightarrow(2+2F_0(1+Bi))T_{i,1}^{n+\frac{1}{2}}-2F_0T_{i,2}^{n+\frac{1}{2}}=F_0T_{i-1,1}^n+(2-2F_0)T_{i,1}^n+F_0T_{i+1,1}^n+2F_0BiT_\infty \\ i=m,j=m\rightarrow-2F_0T_{m,m-1}^{n+\frac{1}{2}}+(2+2F_0(1+Bi))T_{m,m}^{n+\frac{1}{2}}=F_0T_{m-1,m}^n+(2-2F_0(1+Bi))T_{m,m}^n+4F_0BiT_\infty \\ i<m,j=m\rightarrow-2F_0T_{i,m-1}^{n+\frac{1}{2}}+(2+2F_0(1+Bi))T_{m,m}^{n+\frac{1}{2}}=F_0T_{i-1,m}^n+(2-2F_0(1+Bi))T_{m,m}^n+2F_0BiT_\infty \end{cases} \tag{5}$$

It should be pointed out that equations depicted in Eq. 5 are written for the first half step. Nevertheless, for the next half step, similar equations are obtained. In order to avoid reiteration, they are not demonstrated. Finally, when finite equations for every step and grid are written, a system of polynomial equations is achieved which could be shown in the form of tri-diagonal matrices. For instance, the linear system of equations in the form of matrices is as per Eq. 6.

$$\begin{cases} \{T\}^{n+\frac{1}{2}}=\{A\}^{-1}\times\{B\} \\ \{T\}^{n+1}=\{A\}^{-1}\times\{B\} \end{cases} \tag{6}$$

3.3 Solving the inverse problem

In the inverse problem at hand, the strength (Q) of the point heat source is regarded as the unknown parameter. The additional information obtained from transient temperature measurements (Section 2) taken at locations [x, y]=[x_{meas}(T1),…, x_{meas}(T4); y_{meas}(T1),…, y_{meas}(T4)], at times t_i, i=1, 2, …, I, is then used for the estimation of Q=P. The problem introduced by Eqs. 1 and 2 with Q as the unknown and parameterized as P is an inverse heat conduction problem in which the P is to be estimated [19]. According to LM method, the solution of this inverse heat conduction problem for the estimation of the unknown parameter P is based on the minimization of the ordinary least squares norm given by Eq. 7:

$$S(p)=[Y-T(p)]^T[Y-T(p)] \tag{7}$$

Where the superscript T denotes the transpose, and the estimated temperatures $T_i(P)$ are acquired from the solution of the direct problem at the measurement locations [x_{meas}*(T1),…, x_{meas}(T4); y_{meas}(T1),…, y_{meas}(T4)] using the current estimate for the unknown parameter P.*

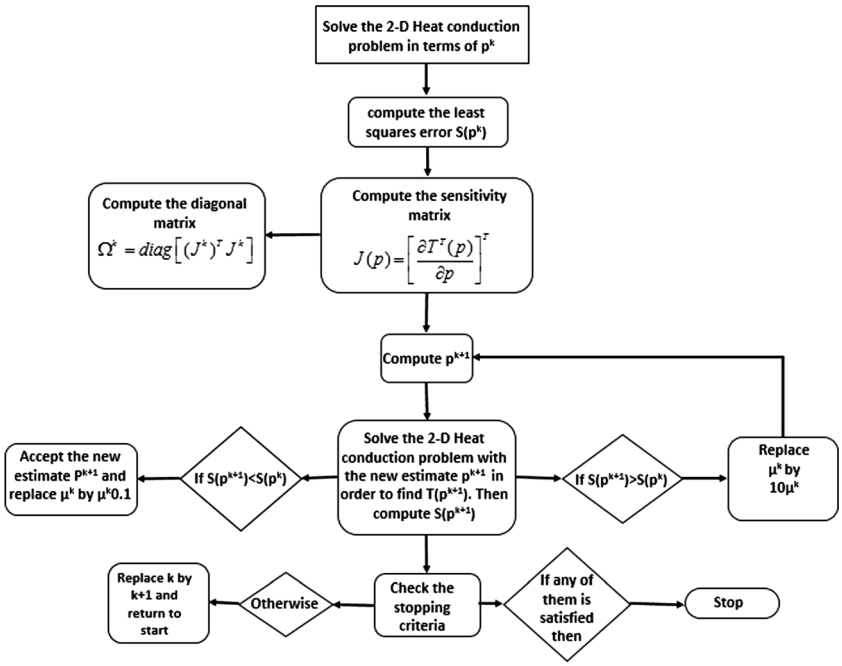

Fig. 4 The computational algorithm flow chart for LM method

The iterative procedure for LM technique To minimize the least squares norm given by Eq. 7, the derivative of $S(P)$ with respect to the unknown parameter is equated to zero. This minimization is represented in matrix notation by equating the gradient of $S(P)$ with respect to the vector of parameter P to zero, that is:

$$\nabla S(p) = 2\left[-\frac{\partial T^T(p)}{\partial p}\right][Y - T(p)] = 0 \tag{8}$$

Finally, by defining the sensitivity or Jacobin matrix as $J(P) = \left[\frac{\partial T^T(P)}{\partial P}\right]^T$, the following iterative procedure is given by LM method to obtain the vector of unknown parameter P [19]:

$$p^{k+1} = p^k + \left[\left(J^k\right)^T J^k + \mu^k \Omega^k\right]^{-1} \left(J^k\right)^T \left[Y - T\left(p^k\right)\right] \tag{9}$$

The purpose of the matrix term $\mu^k \Omega^k$, included in Eq. 9, is to damp oscillations and instabilities due to the ill-conditioned

Table 4 Obtained values of total, received to W.P, and portion of energy transferred to W.P on fixed voltage V=80 v

Number of experiment	Discharge current (A)	Pulse duration (μs)	Energy transferred To the W.P (mJ)	Total energy (mJ)	F_c
1	2	12.8	0.12	2.048	0.058
2	2	25	0.325	4	0.08
3	2	50	0.477	8	0.05
4	2	100	0.615	16	0.038
5	4	12.8	0.221	4.096	0.05
6	4	25	1.325	8	0.16
7	4	50	4.423	16	0.27
8	4	100	9.362	32	0.29
9	8	12.8	0.319	8.192	0.03
10	8	25	2.385	16	0.149
11	8	50	6.49	32	0.202
12	8	100	23.98	64	0.374
13	12	12.8	1.347	12.288	0.10
14	12	25	5.429	24	0.226
15	12	50	14.565	48	0.303
16	12	100	44.261	96	0.461

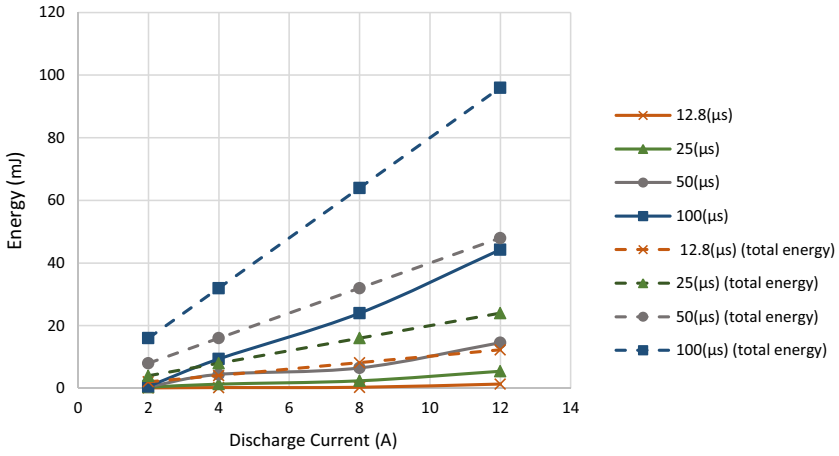

Fig. 5 Total discharge energy and energy transferred to the W.P vs. discharge current at various levels of pulse duration

character of the problem ($|J^TJ| \approx 0$), by making its components large as compared to those of J^TJ if necessary. The damping parameter μ^k is made large in the beginning of the iterations, since the problem is generally ill-conditioned in the region around the initial guess used for the iterative procedure, which can be quite far from the exact parameter P. The parameter μ^k is then gradually reduced as the iteration procedure advances to the solution of the parameter estimation problem [19].

The stopping criteria for LM technique The following criteria were suggested by Dennis and Schnabel [22] to stop the iterative procedure of the LM method given by Eq. 9:

$$\text{(i)} \quad S\left(P^{k+1}\right) < \varepsilon_1 \tag{10}$$

$$\text{(ii)} \quad \left\| \left(J^k\right)^T \left[Y - T\left(P^k\right)\right] \right\| < \varepsilon_2 \tag{11}$$

$$\text{(iii)} \quad \left\| P^{k+1} - P^k \right\| < \varepsilon_3 \tag{12}$$

where ε_1, ε_2, and ε_3 are user prescribed tolerances and $\|.\|$ is the vector Euclidean norm, i.e., $\|x\| = (x^Tx)^{\frac{1}{2}}$, where the superscript T denotes transpose.

The criterion given by Eq. 10 tests if the least squares norm is sufficiently small, which is expected to be in the neighborhood of the solution for the problem. Similarly, Eq. 11 checks if the norm of the gradient of $S(P)$ is sufficiently small, since it is expected to vanish at the point where $S(P)$ is minimum. Although such condition of vanishing gradient is also valid for maximum and saddle points of $S(P)$, the LM method is very unlikely to converge to such points. The last criterion given by Eq. 12 results from the fact that changes in the vector of the parameter are very small when the method has converged.

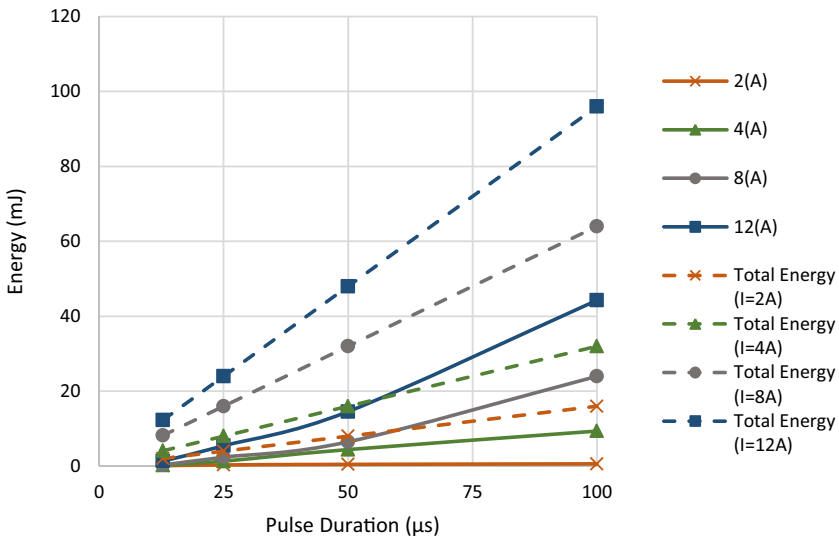

Fig. 6 Total discharge energy and the energy transferred to the W.P vs. pulse duration at various levels of discharge current

4 Results and discussions

A computer code in MATLAB script software based on the computational algorithm depicted as a flow chart in Fig. 4 was written for calculation of unknown power transferred to the workpiece. In other words, with compiling the script, the unknown power transferred to the workpiece during each experiment is evaluated.

Furthermore and having the quantities of power transferred to the workpiece determined, Eqs. 10 and 11 are applied and the values of the energy transferred to the workpiece and the total discharge energy for each set up are determined, respectively. Afterwards, portion of energy (F_c) is obtained using Eq. 15. Table 4 lists the determined F_c for each experiment where discharge current and pulse durations are varied and voltage is kept constant. This inverse heat transfer method could be used to estimate the energy transferred to the workpiece for any machining conditions during EDM process.

$$E_w = P_w \cdot T_{\text{on}} \tag{13}$$

$$E_{\text{total}} = \int_0^{ptT_{\text{on}}} V_{\text{avg}} . I_{\text{dis}} . dt \tag{14}$$

$$F_c = \frac{E_w}{E_{\text{total}}} \tag{15}$$

Figures 5 and 6 illustrate the effects of discharge current and pulse duration on total energy and the energy delivered to the workpiece. It could be comprehended that by increasing discharge current and pulse duration, both the total energy and the energy transferred to workpiece have increased, for the reason that according to Eq. 11, there exists a direct relationship between discharge energy and machining parameters.

Furthermore, Figs. 7 and 8 demonstrate the effect of discharge current and pulse duration on portion of energy transferred to the workpiece, i.e., F_c. As it is apparent, the joint effect of discharge current and pulse duration, i.e., the discharge energy on F_c, is stronger than the separate effects of

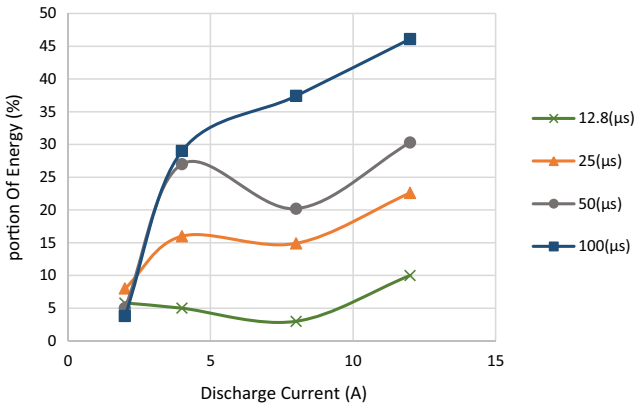

Fig. 7 Portion of energy vs. discharge current at various levels of pulse duration

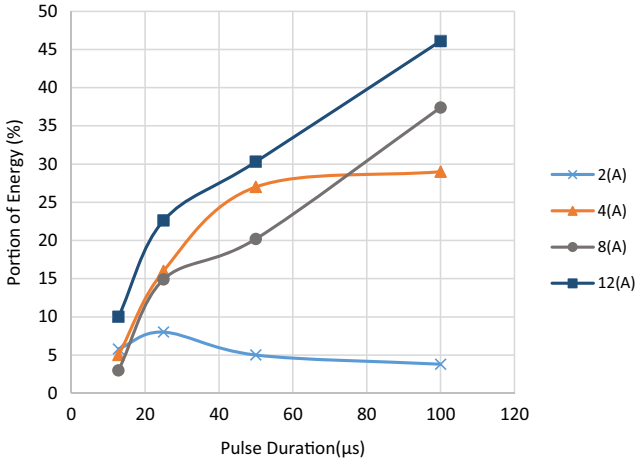

Fig. 8 Portion of energy vs. pulse duration at various levels of discharge current

the each parameter on F_c. In other words, at low discharge currents, the pulse duration has a slight effect on F_c, while at high discharge currents, pulse duration has much more stronger effect on F_c. Meanwhile, at short pulse durations, the discharge current has a low impact on F_c, while at long pulse durations, the effect is much more intense. This is owing to the fact that at low intensities of discharge current, the density of plasma channel (heat source) is low; therefore, an increase in pulse duration while making the heat source more stable has low impact on F_c. However, at high intensities of discharge current, the density of plasma channel, i.e., heat source, becomes much higher, which means thermal energy is being generated at a high rate. Plus, the increase of pulse duration results in a steady heat source. Therefore, the dense heat source has significant thermal energy transfer rate and sufficient time for conducting it. As the result, more energy is being transferred to the workpiece; thus, the increase of the F_c.

On the other hand, at short pulse durations, an increase in current intensities amplifies the energy density of the heat source. However, the discharges occur at high frequencies due to short pulses and therefore, the heat source is unstable and there is not enough time for conducting the energy which means the impact of current is insignificant. Furthermore, at long pulse durations, the heat source has the adequate time interval to deliver its thermal energy to the workpiece; consequently, with the increase of current intensity, the portion of energy transferred to workpiece ascends.

5 Conclusions

This work has made use of the Levenberg-Marquardt technique of parameter estimation alongside temperature measurements using embedded thermocouple method in order to solve the two-dimensional inverse heat conduction with a point heat source in a rectangular problem, consequently determining the

energy transferred to the workpiece in EDM process. It can be concluded that:

1. The portion of energy transferred to the workpiece (F_c) is a function of discharge current and pulse duration. For lower energy zones, F_c has a span of 5–18 %. While, for medium and high energy zones in EDM processes, F_c varies from 18 to 45 %.
2. F_c reaches its maximum value of 45 % for current study, which reveals that most of the total discharge energy is lost through convection and radiation to the dielectric fluid and by conduction via the tool (anode).
3. The joint effect of pulse duration and discharge current on F_c is superior to their individual effect on F_c. Furthermore, discharge current has stronger impact on F_c than pulse duration.
4. The use of inverse heat transfer techniques warrant the determination of the heat source from the knowledge of temperature and thermo-mechanics of any machining process; therefore, this method can be applied for other machining processes as well.
5. This method can be generalized for other simple geometries on two- and three-dimensional spaces. The conversion can be achieved by replacing the partial differential equation of heat transfer for the respective model in proper system of coordinates.

Compliance with ethical standards This research received no specific grant from any funding agency in the public, commercial, or not-for-profit sectors and there are no conflicts of interest to the authors' recollection. Moreover, both authors assure that there were no human participants involved in this research and the whole research was the result of the research and work done by the two authors listed in the title page. In addition, no animals were used or involved while conducting the experiments for this research.

References

1. Yeo SH, Kurnia W, Tan PC (2008) Critical assessment and numerical comparison of electro-thermal models in EDM. J Mater Process Technol 203:241–251
2. Izquierdo B, Sánchez JA, Plaza S, Pombo I, Ortega N (2009) A numerical model of the EDM process considering the effect of multiple discharges. Int J Mach Tools Manuf 49:220–229
3. Snoeys R, Van Dijck F, Peters J (1972) Plasma channel diameter growth affects stock removal in EDM. CIRP Annals 21:39–40
4. Van Dijck FS, Dutré WL (1974) Heat conduction model for the calculation of the volume of molten metal in electric discharges. J Phys D Appl Phys 7:899
5. Beck JV (1981) Large time solutions for temperatures in a semi-infinite body with a disk heat source. Int J Heat Mass Transf 24: 155–164
6. Beck JV (1981) Transient temperatures in a semi-infinite cylinder heated by a disk heat source. Int J Heat Mass Transf 24:1631–1640
7. Tariq Jilani S, Pandey PC (1983) An analysis of surface erosion in electrical discharge machining. Wear 84:275–284
8. Pandey PC, Jilani ST (1986) Plasma channel growth and the resolidified layer in edm. Precis Eng 8:104–110
9. Singh H, Shukla DK (2012) Optimizing electric discharge machining parameters for tungsten-carbide utilizing thermo-mathematical modelling. Int J Therm Sci 59:161–175
10. DiBitonto DD, Eubank PT, Patel MR, Barrufet MA (1989) Theoretical models of the electrical discharge machining process. I. A simple cathode erosion model. J Appl Phys 66:4095–4103
11. Eubank PT, Patel MR, Barrufet MA, Bozkurt B (1993) Theoretical models of the electrical discharge machining process. III. The variable mass, cylindrical plasma model. J Appl Phys 73:7900–7909
12. Kunieda M, Lauwers B, Rajurkar KP, Schumacher BM (2005) Advancing EDM through fundamental insight into the process. CIRP Ann Manuf Technol 54:64–87
13. Joshi SN, Pande SS (2010) Thermo-physical modeling of die-sinking EDM process. J Manuf Process 12:45–56
14. Singh H (2012) Experimental study of distribution of energy during EDM process for utilization in thermal models. Int J Heat Mass Transf 55:5053–5064
15. Zahiruddin M, Kunieda M (2012) Comparison of energy and removal efficiencies between micro and macro EDM. CIRP Ann Manuf Technol 61:187–190
16. Fonda P, Wang Z, Yamazaki K, Akutsu Y (2008) A fundamental study on Ti–6Al–4V's thermal and electrical properties and their relation to EDM productivity. J Mater Process Technol 202:583–589
17. H.D. Baehr, K. Stephan, H.D. (2006) Baehr, Heat conduction and mass diffusion, Heat Mass Transfer 105-251
18. Beck JV, Blackwell B, St Clair CR (1985) Inverse heat conduction: ill-posed problems. A Wiley-Interscience, New York
19. Ozisik MN, Orlande HRB (2000) Inverse heat transfer: fundamentals and applications. Taylor & Francis, London
20. Taler J, Duda P (2006) Solving direct and inverse heat conduction problems. Springer, Verlag Berlin Heidelberg
21. Debnath L (2007) Linear partial differential equations for scientists and engineers. Springer, Verlag Berlin Heidelberg
22. Dennis JE Jr, Schnabel RB (1996) Numerical methods for unconstrained optimization and nonlinear equations. Siam, Philadelphia